FINAL REPORT

DOE Project No. DE-FG36-02ID14415

DEVELOPMENT AND ANALYSIS OF FAST, APPROXIMATE, 3D ALGORITHMS FOR INTERPRETATION OF MULTI-COMPONENT INDUCTION LOGGING DATA

PI: Dr. David L. Alumbaugh

Formerly:
University of Wisconsin-Madison
Department of Civil and Environmental Engineering
Geological Engineering Program
2258 Engineering Hall
1415 Engineering Drive
Madison, WI 53706

Currently:
Schlumberger/EMI Technology Center
1301 S. 46th St. #300
Richmond, CA 94804

Table of Contents

1.0 Executive Summary

This report addresses the effects of electrical anisotropy on the 3D inversion of single-well induction logging data when anisotropy is not considered. Of concern are possible artifacts that may lead to an incorrect interpretation of the formation about the borehole. Comparison is made of 3D isotropic inversion on a suite of model data, with and without anisotropy, consisting of an infinite layer and layer terminated at the borehole. In both cases, the layer dip (or well deviation) is varied. Inversion of the anisotropic data result in an overestimate of the layer conductivity, and the lateral extent of the layer about the borehole.

2.0 Description of the Proposed Work

Inductive resistivity logging has long been an important technology to oil and gas producers because of the sensitivity of electrical resistivity to geological structure and variations in reservoir fluids. Electrical resistivity data from well logs is often used in geologically describing reservoirs, locating fractures, and selecting producing intervals in wells. Unfortunately, commercial tools of this type are not commonly used by geothermal developers, because they are not built to withstand the hostile high temperature environment found in geothermal boreholes. In addition, commercial logging tools that can locate, orient, and assess fracture zones in terms of their geometry, extent, and production potential at large distances from the well axis do not exist. If available, this capability could guide drilling programs and optimize the placement of production and injection wells resulting in fewer dry holes and substantial cost savings in field development.

A few years ago, the DOE and the California Energy Commission (CEC) funded ElectroMagnetic Instruments, Inc. (EMI) of Richmond, California, to build a prototype induction-logging device that will provide downhole electromagnetic identification and characterization of geothermal resources. The resulting ‘Geo-BILT’ successfully collected data in California oilfields and attempted to collect data in the hot, downhole environments present at the Dixie Valley and Geysers geothermal fields in Nevada and California, respectively. Because wells intersect production zones at oblique angles, and three-dimensional (3D) variability exists within geothermal reservoirs, standard induction logging analysis that assumes two-dimensional (2D) cylindrical symmetry about the borehole will provide unreliable interpretations. Inversion algorithms that perform “exact” 3D inversions of multi-component data do exist. However, massively parallel computing is necessary to arrive at timely solutions. Since massively parallel computing is neither easily accessible nor practical for many industry and field applications, a “fast” imaging scheme, which can be implemented on standard computing hardware, is required. In addition, fractured-production zones likely exhibit electrical anisotropy where the resistivity parallel to the fracture is different than that perpendicular to the zone. This can cause significant distortions in the measured fields that are not accounted for in current 3D isotropic inversion algorithms.

We proposed a three-step process to address the problem of 3D induction logging in a geothermal reservoir environment. The first step was to determine the need of a three-dimensional inversion algorithm that accounts for the presence of anisotropy by

applying an available 3D isotropic inversion algorithm to synthetic data generated in the presence of anisotropy. The need for an anisotropic inversion would be assessed from the isotropic inversion results by the nature and size of artifacts produced by the anisotropy. The second step was to develop an approximate inversion algorithm that provides the computational speed necessary to invert multi-component borehole electromagnetic induction data in a few hours rather than days. The two-step algorithm was to be based on a non-linear inversion to recover a layered anisotropic (or isotropic if it is determined to be so) model, followed by a single-iterate Gauss-Newton scheme to image 3D heterogeneity. The final step was to assess the accuracy and applicability of the scheme by testing it on synthetic data sets generated with a 3D forward modeling algorithm and by applying it to data collected with the Geo-BILT tool in two different geothermal reservoirs. Unfortunately, due to the fact that the PI took a leave of absence soon after the project was funded and soon after left the university for industry, and the student performing the work left the University of Wisconsin a year after the PI to pursue graduates studies elsewhere, only the first task was completed. The second task consisting of the development of an approximate algorithm was initiated but never completed, while the third task could not even be started as the Dixie Valley data collected with the Geo-BILT showed little evidence of any structure at all, and data collected at the Geysers was too noisy due to the fact that the well was producing while data were being collected. Thus this report, the results of which were presented at the 2004 Annual Meeting of the Society of Exploration Geophysicists, outlines the findings only of the first task of the proposed work.

3.0 Results

3.1 Introduction

With the advent of greater computational capabilities and faster, more accurate, induction logging acquisition systems, comes the possibility of generating 3D images of the region surrounding the well bore. This has great potential in oil and geothermal reservoir characterization in terms of delineating bypassed production zones, as well as providing additional data that leads to a better exploration strategy. The data required to provide the 3D images include 3-component measurements of the magnetic field generated by at least one, if not three orthogonally oriented loop sources. Three-dimensional imaging and inversion algorithms are now available (e.g., Newman and Alumbaugh, 1997; Zhdanov et al., 2002), and recent numerical studies have employed these algorithms to show potential of this imaging technique (Alumbaugh and Wilt, 2001; Zhdanov et al., 2004). However, many target zones of interest exhibit electrical anisotropy where the resistance to current flow is directionally dependent. Examples of this include interbedded sand-shale sequences or turbidite deposits in oil reservoirs (Nekut, 1994), and stress-oriented fracture zones in geothermal fields. The aforementioned imaging algorithms assume isotropic materials, and thus cannot account for anisotropy. This paper will present results that show the effect of electrical anisotropy on 3D isotropic imaging, and will determine the level of error that arises in the images due to the introduction of this parameter. The focus will be on simple anisotropic targets such as fracture zones found within geothermal reservoirs.

3.2 Forward Modeling Studies

A suite of calculations was performed on targets consisting of an infinite layer and a half-infinite layer within a background whole space (

Figure 1). Variations in the models included the layer dip-angle which varied from 0^o to 60^o, and the conductivity of the layer in the direction perpendicular to the bedding plane, which was 5 or 20 times less than that of the conductivity in the parallel to-bedding direction. In each case, the layer thickness is 3.5 m and the layer-parallel conductivity is 1 S/m., with the background conductivity fixed at 0.1 S/m. Regarding the tool configuration, the transmitter-receiver separation is 2 m, and the frequency is 4 kHz. This resembles that of an existing multi-component induction logging tool, the GeoBILT (EMI, 1998). Calculations were made at 0.5 m intervals along the borehole axis and extended to approximately 10 m above and below the borehole-layer intersection. Calculation of the x-, y- and z-component field is made for each of the x-, y- and z-directed sources, constituting nine field calculations for each depth.

Calculations were performed using a 3D finite difference electromagnetic modeling algorithm developed by Newman and Alumbaugh (1995) with the ability to accommodate anisotropy in conductivity. Infinite layer calculations were compared against a 1D transverse anisotropic code (Lu and Alumbaugh, 2001) to ensure appropriate mesh gridding.

Sample results presented in Figure 2 of the coaxial, coplanar and coaxial null-coupled responses for a 0^o and 60^o-dipping layer show deviations in amplitude caused by anisotropy. This is a result of the near-well sensitivity changing as the angle between the tool axis and the conductivity tensor changes (Lu and Alumbaugh, 2001; Tompkins et al., 2004). As a result of the anisotropy altering the total field amplitude relative to the isotropic case, assumptions used in inverting multi-component data for near-well formation properties can result in error. For example, if only the coaxial data are employed, the formation conductivity will be underestimated, and the magnitude of the error will depend on the magnitude of the anisotropy coefficient ($\lambda = \sqrt{\sigma_h/\sigma_v}$) and the dip angle of the formation.

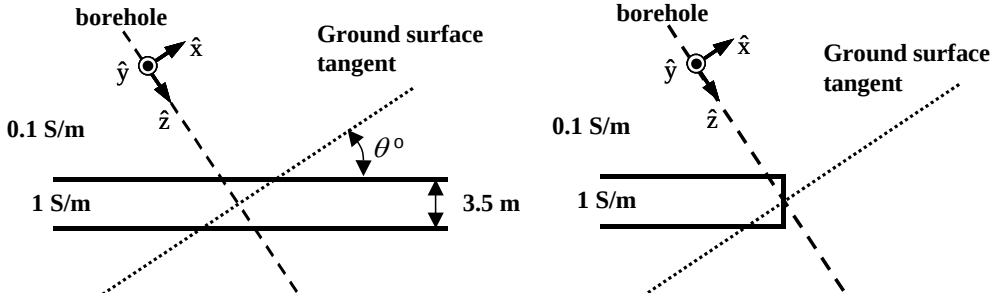

Figure 1: Schematics of models simulated.

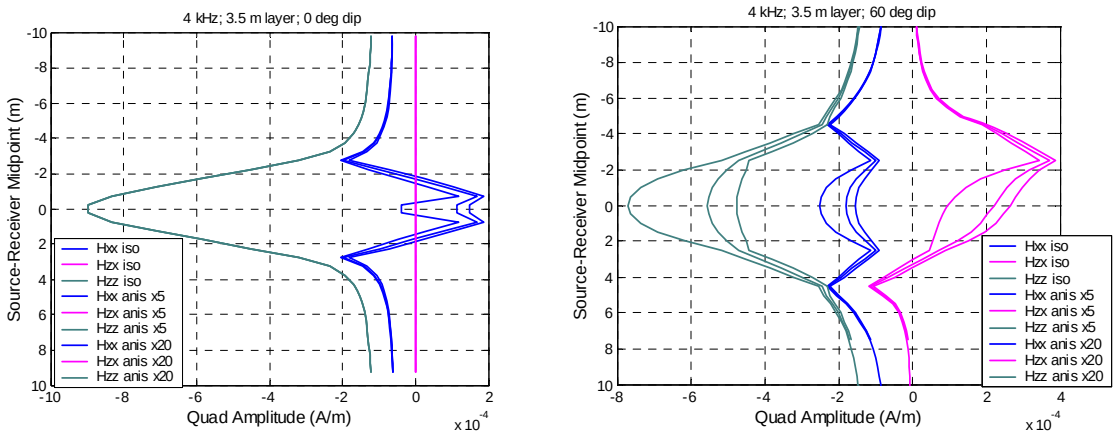

Figure 2: Forward model results.

3.3 Three-Dimensional Isotropic Inversion of Anisotropic Data

The forward model data were inverted using the 3D Gauss-Newton inversion scheme developed by Newman and Alumbaugh (1997). This scheme employs regularization that imposes smoothness on the conductivity reconstructions, where the regularization parameter is updated at each iteration based upon the updated Jacobian.

The inversion was applied to the three component data generated by each of the axially and the two horizontally aligned sources, yielding a total of 9 data components to be inverted for each depth. A uniform grid over the inversion domain extended 4 m above and below the top transmitter and bottom receiver positions, respectively, and extended horizontally out to 8 m. Vertical cell spacing is 0.5 m, equal to the measurement interval, and horizontal cell spacing is 0.8 m. The same mesh was used for all models. The starting model was a 0.1 S/m whole-space. The size of the modeling mesh was 36 by 36 by 65 cells with an inversion domain of 20 by 20 by 51 cells. Computations were performed on 96 high performance RISC nodes on the IBM SP parallel computer facilities available through the National Energy Research Super Computing center located at Lawrence Berkeley Laboratory.

Inversion results for the two models in
Figure 1, having 0^o and 30^o dip, are presented in Figure 3-Figure 14. For each case, isotropic and anisotropic case, where the horizontal conductivity is 20 times that of the vertical, are compared. Figure 3 shows the inverted conductivity distribution for 0^{o-} dipping infinite layer, with the resultant data fit shown in Figure 4. Figure 5 shows the misfit (sum of square error) and the regularization parameter versus iteration. Results are similarly presented for 30^o-dipping infinite layer (Figure 6 through Figure 8), 0^o-dipping half-infinite layer (Figure 9 through Figure 11) and 30^o-dipping half-infinite layer (Figure 12 through Figure 14) models.

In all cases, several observations are made. The conductivity estimate of the anisotropic layer is overestimated, and the distribution is moved closer, or localized, to the borehole. Additionally, the anisotropic data require considerably more iterations to achieve a misfit comparable to the isotropic data. The inversion results for the isotropic

models adequately resolve the layer conductivity distribution; though, conductivity estimates tend to be overestimated around borehole. This is likely due to the fact that only one receiver-offset and frequency was employed, affecting the resolution. What is observed in the anisotropic models is this effect of overestimating and localizing the conductivity estimates is considerably enhanced. As seen from the regularization parameter plots, the smoothness constraints for the inversions of the anisotropic data are approximately the same, if not slightly higher (meaning more constrain to produce a smooth conductivity estimate), than for the isotropic data. Therefore, the inversion regularization is ruled out as a cause for the 'roughness' in the conductivity estimates for the anisotropic models.

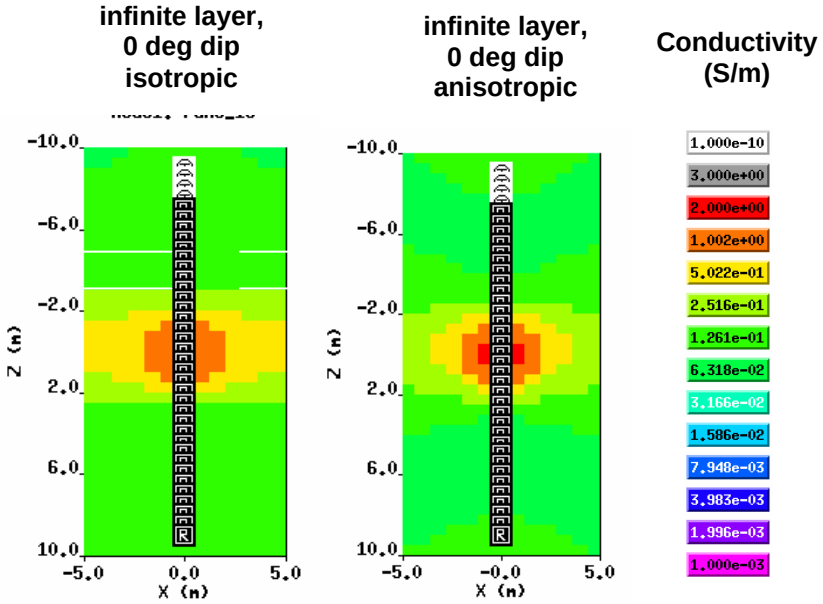

Figure 3: Inversion results for the 0^{o} dip, infinite layer. a) Isotropic layer. b) Anisotropic layer.

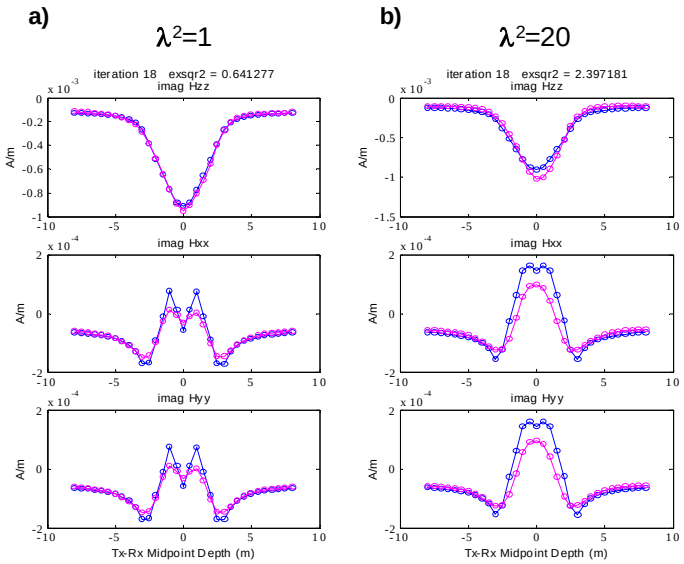

Figure 4: Inversion data fit for the horizontal, infinite layer. a) Isotropic layer. b) Anisotropic layer.

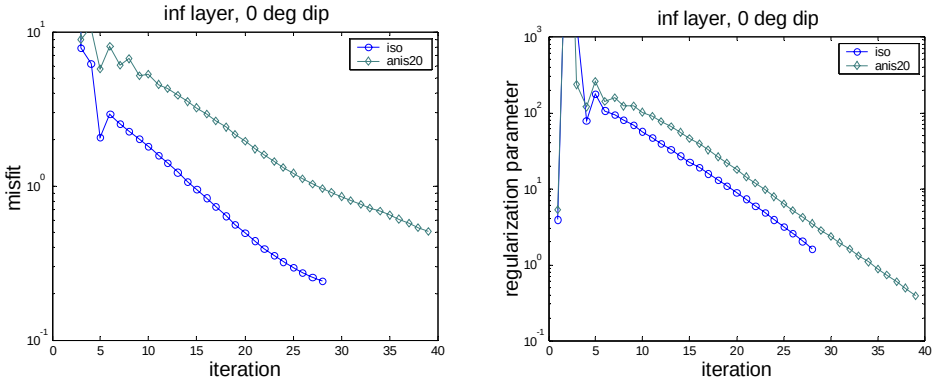

Figure 5: a) misfit and b) regularization versus iteration for the horizontal, infinite layer.

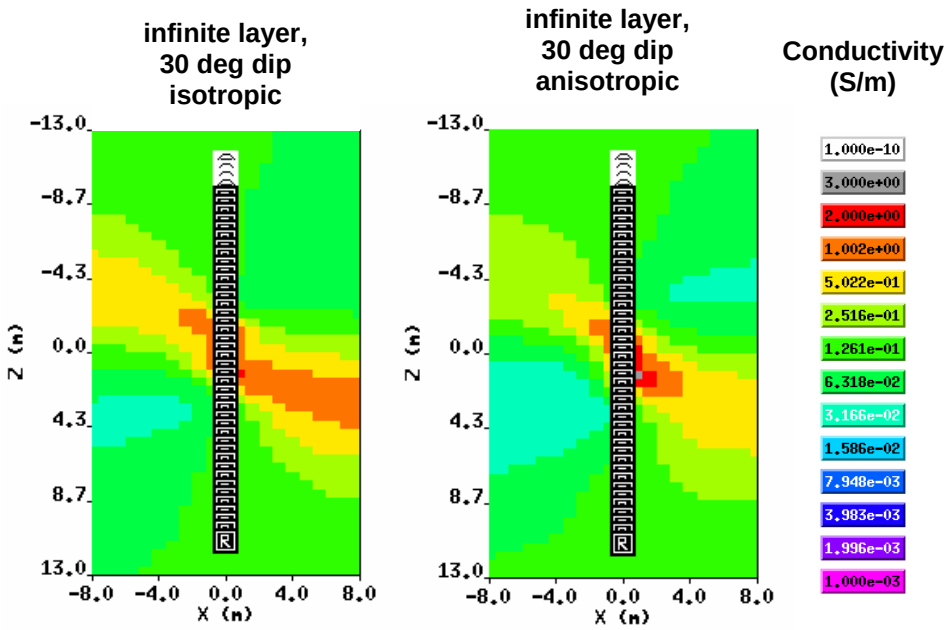

Figure 6: Inversion results for the 30^{o} dip, infinite layer. a) Isotropic layer. b) Anisotropic layer.

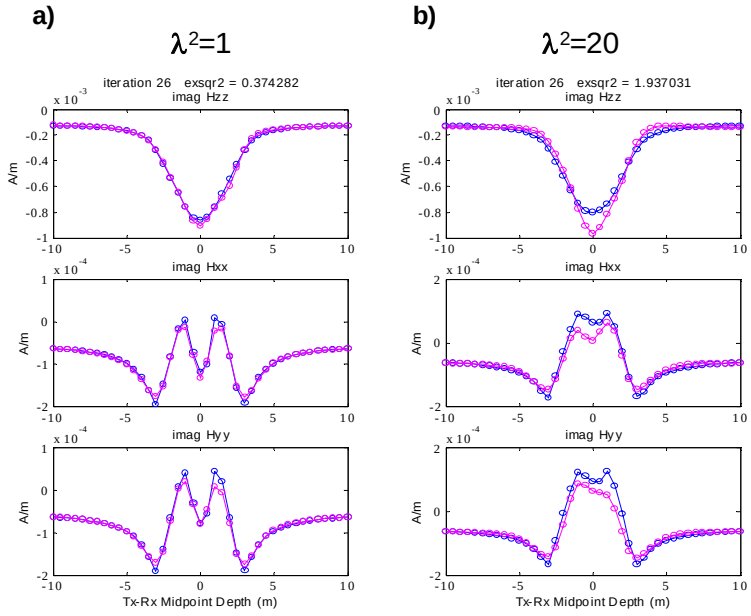

Figure 7: Inversion data fit for the 30^{o} dip, infinite layer. a) Isotropic layer. b) Anisotropic layer.

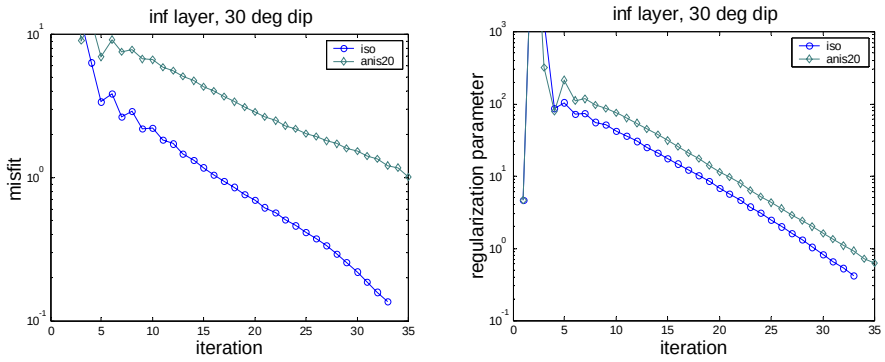

Figure 8: a) misfit and b) regularization versus iteration for the 30^{o} dip, infinite layer.

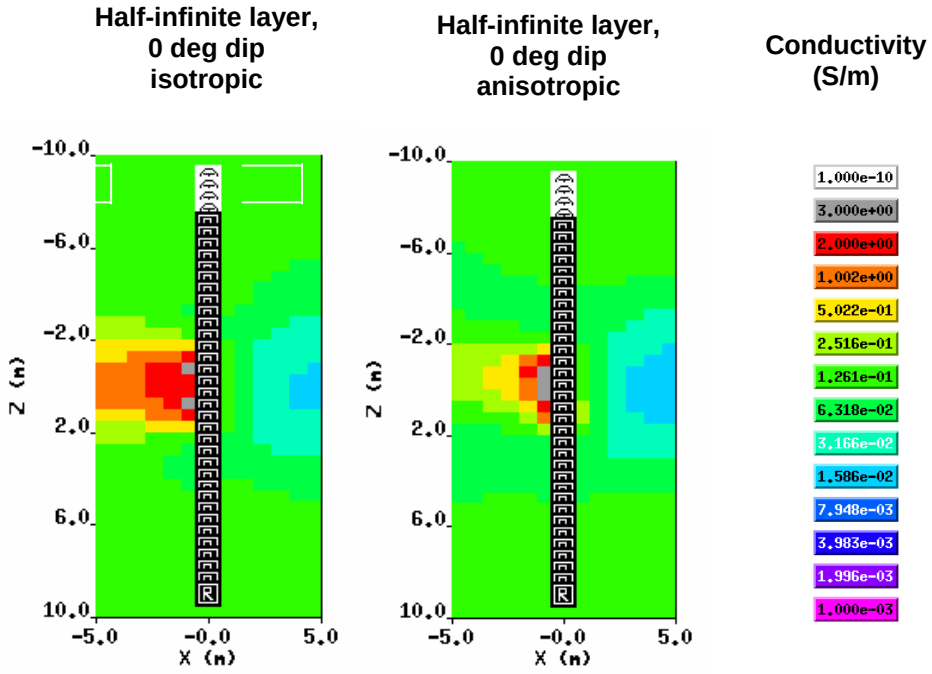

Figure 9: Inversion results for the 0^{o} dip, half-infinite layer. a) Isotropic layer. b) Anisotropiclayer.

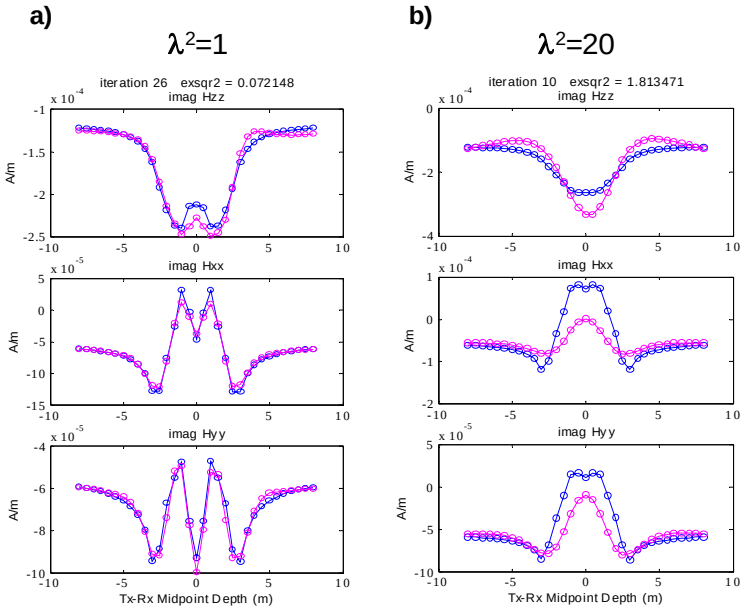

Figure 10: Inversion data fit for the horizontal, terminated layer. a) Isotropic layer. b) Anisotropic layer.

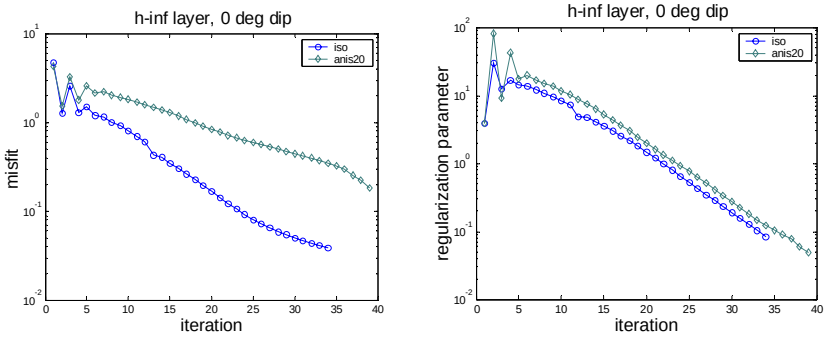

Figure 11: a) misfit and b) regularization versus iteration for the horizontal, half-infinite layer.

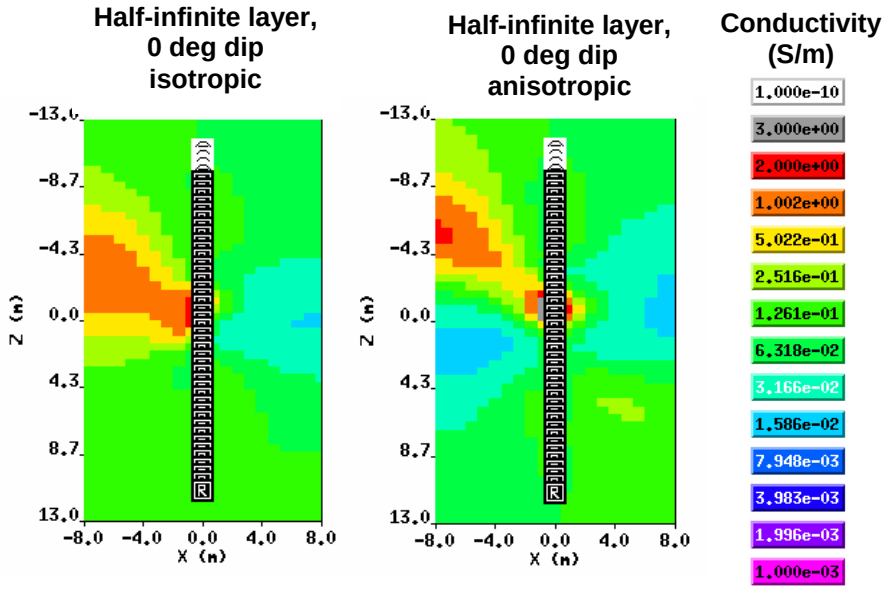

Figure 12: Inversion results for the 30^{o} dip, half-infinite layer. a) Isotropic layer. b) Anisotropic layer.

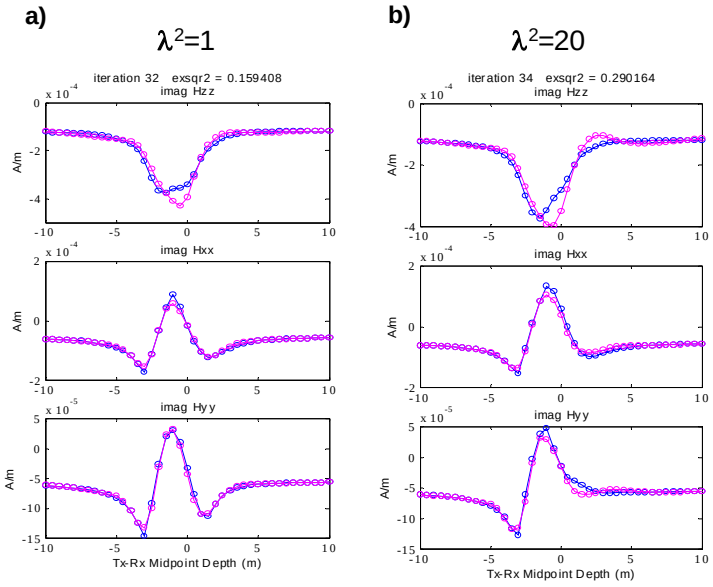

Figure 13: Inversion data fit for the 30^{o} dip, terminated layer. a) Isotropic layer. b) Anisotropic layer.

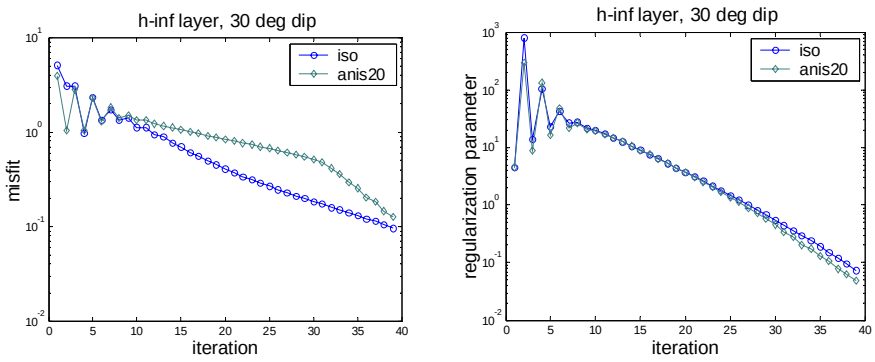

Figure 14: a) misfit and b) regularization versus iteration for the 30^{o} dip, infinite layer.

4.0 Conclusions

The effects of anisotropy on standard induction logging in a simple model is well understood, with the resultant artifact being an over estimation of the layer resistivity. We've presented anisotropic effects on 3D induction logging in more complex models. The apparent effects are conductivities estimates that are over estimated and become more confined about the borehole. We attribute these effects as artifacts caused by the anisotropy.

5.0 References

Alumbaugh, D.L., and Wilt, M.J., 2001, A numerical sensitivity study of three-dimensional imaging from a single borehole, Petrophysics, v. 42, 19-31.

EMI, 1998, Development of an Extended Induction Logging Tool for Geothermal Exploration and Field Development, Proposal submitted to the California Energy Commision under the Pier I program.

Lu, X., and Alumbaugh, D.L., 2001, One-dimensional inversion of three-component induction logging in anisotropic media, expanded abstracts, Society of Exploration Geophysicists 71st Annual Meeting, San Antonio, Texas.

Nekut, A.G., 1994, Anisotropy Induction Logging, Geophysics, v. 59, 3, 345-350.

Newman, G.A., and Alumbaugh, D.L., 1995, Frequency-domain modeling of airborne electromagnetic responses using staggered finite differences, Geophysical Prospecting, v. 43, 1021-1042.

Newman, G.A., and Alumbaugh, D.L., 1997, Three-dimensional massively parallel inversion – I. Theory, Geophys. J. Int., 128, 345-354.

Tompkins, M.J., Alumbaugh, D.L., Stanley, D.T., and Lu, X., 2004, Numerical analysis of near-borehole and anisotropic layer effects on the response of multicomponent induction logging tools, Geophysics, v. 69, 1, 140-151.